

NASA/TM-2010-216858



CFL3D Contribution to the AIAA Supersonic Shock Boundary Layer Interaction Workshop

*C. L. Rumsey
Langley Research Center, Hampton, Virginia*

October 2010

NASA STI Program . . . in Profile

Since its founding, NASA has been dedicated to the advancement of aeronautics and space science. The NASA scientific and technical information (STI) program plays a key part in helping NASA maintain this important role.

The NASA STI program operates under the auspices of the Agency Chief Information Officer. It collects, organizes, provides for archiving, and disseminates NASA's STI. The NASA STI program provides access to the NASA Aeronautics and Space Database and its public interface, the NASA Technical Report Server, thus providing one of the largest collections of aeronautical and space science STI in the world. Results are published in both non-NASA channels and by NASA in the NASA STI Report Series, which includes the following report types:

- **TECHNICAL PUBLICATION.** Reports of completed research or a major significant phase of research that present the results of NASA programs and include extensive data or theoretical analysis. Includes compilations of significant scientific and technical data and information deemed to be of continuing reference value. NASA counterpart of peer-reviewed formal professional papers, but having less stringent limitations on manuscript length and extent of graphic presentations.
- **TECHNICAL MEMORANDUM.** Scientific and technical findings that are preliminary or of specialized interest, e.g., quick release reports, working papers, and bibliographies that contain minimal annotation. Does not contain extensive analysis.
- **CONTRACTOR REPORT.** Scientific and technical findings by NASA-sponsored contractors and grantees.

- **CONFERENCE PUBLICATION.** Collected papers from scientific and technical conferences, symposia, seminars, or other meetings sponsored or co-sponsored by NASA.
- **SPECIAL PUBLICATION.** Scientific, technical, or historical information from NASA programs, projects, and missions, often concerned with subjects having substantial public interest.
- **TECHNICAL TRANSLATION.** English-language translations of foreign scientific and technical material pertinent to NASA's mission.

Specialized services also include creating custom thesauri, building customized databases, and organizing and publishing research results.

For more information about the NASA STI program, see the following:

- Access the NASA STI program home page at <http://www.sti.nasa.gov>
- E-mail your question via the Internet to help@sti.nasa.gov
- Fax your question to the NASA STI Help Desk at 443-757-5803
- Phone the NASA STI Help Desk at 443-757-5802
- Write to:
NASA STI Help Desk
NASA Center for AeroSpace Information
7115 Standard Drive
Hanover, MD 21076-1320

NASA/TM-2010-216858



CFL3D Contribution to the AIAA Supersonic Shock Boundary Layer Interaction Workshop

C. L. Rumsey
Langley Research Center, Hampton, Virginia

National Aeronautics and
Space Administration

Langley Research Center
Hampton, Virginia 23681-2199

October 2010

Acknowledgments

The author would like to thank Dr. N. Georgiadis of NASA Glenn Research Center for generously providing grids.

The use of trademarks or names of manufacturers in this report is for accurate reporting and does not constitute an official endorsement, either expressed or implied, of such products or manufacturers by the National Aeronautics and Space Administration.

Available from:

NASA Center for AeroSpace Information
7115 Standard Drive
Hanover, MD 21076-1320
443-757-5802

Abstract

This paper documents the CFL3D contribution to the AIAA Supersonic Shock Boundary Layer Interaction Workshop, held in Orlando, Florida in January 2010. CFL3D is a Reynolds-averaged Navier-Stokes code. Four shock boundary layer interaction cases are computed using a one-equation turbulence model widely used for other aerodynamic problems of interest. Two of the cases have experimental data available at the workshop, and two of the cases do not. The effect of grid, flux scheme, and thin-layer approximation are investigated. Comparisons are made to the available experimental data. All four cases exhibit strong three-dimensional behavior in and near the interaction regions, resulting from influences of the tunnel side-walls.

1 Introduction

Shock boundary layer interaction (SBLI) is a complex supersonic fluid dynamic phenomenon of relevance in many applications of aerodynamic interest, particularly for supersonic inlet flows. The shock can cause boundary layer separation, which is typically an unsteady phenomenon. Fig. 1 shows a schematic diagram of a SBLI in 2-D. The angle θ of the shock-generating plate defines the strength of the oblique shock wave (the larger θ , the stronger the shock). The oblique shock wave extends down to the lower wall, where it interacts with the oncoming turbulent boundary layer. The computation of SBLI cases has been a focus of the CFD community for many years [1].

In January 2010, a SBLI workshop was held in conjunction with the American Institute of Aeronautics and Astronautics (AIAA) 48th Aerospace Sciences Meeting in Orlando, Florida. The purposes of the workshop were (1) to assess the state-of-the-art computational methods for predicting turbulent SBLI flows, (2) to provide an impartial forum for evaluating the effectiveness of current computer codes and modeling techniques using Navier-Stokes solvers, and (3) to identify areas needing research and development. Several papers came out subsequently, describing the workshop, its results, and lessons learned [2–5]. The reader is referred to these papers for additional details regarding the workshop that are not covered here.

This paper documents a particular submission to the workshop: that of the structured Reynolds-averaged Navier-Stokes (RANS) code CFL3D [6]. The first part of the paper briefly describes the numerical method. Then, a short description of the experiments is provided. Results are then given for four different cases and conclusions are drawn.

2 Numerical Method

CFL3D is a multi-zone compressible Navier-Stokes CFD code in wide use in U.S. industry. It uses point-matched, patched, or overset grids, and employs local time step scaling, grid sequencing, and multigrid to accelerate convergence to steady state. A time-accurate capability is also available, but for all the SBLI cases only steady-state simulations were performed.

CFL3D is a finite volume method. It uses third-order upwind-biased spatial differencing on the convective and pressure terms, and second-order differencing on the viscous terms; it is globally second-order spatially accurate. Both flux vector splitting (FVS) [7] and flux difference splitting (FDS) [8] are available to obtain fluxes at the cell faces. Unless otherwise noted, for all of the computations in this paper, FVS was used due to its greater robustness for strong shock cases. The code is advanced in time with an implicit three-factor approximate factorization method. For most of the applications in this paper, the thin-layer form of the Navier-Stokes equations was solved, with viscous terms active in each of the three coordinate directions in computational space (i.e., viscous cross-derivative terms were neglected). Recently, full Navier-Stokes capability has been added to CFL3D; this capability was exercised for one of the cases to show its effect.

Table 1. Summary of the Experimental Cases

Organization	θ , deg.	M_∞	T_0 , K	p_0 , kPa	Re_θ	status
IUSTI (UFAST)	8.0	2.25	293	50.5	6900	open
UM (CCAS)	7.75	2.75	293	101	6600	open
UM (CCAS)	10.0	2.75	293	101	6600	blind
UM (CCAS)	12.0	2.75	293	101	6600	blind

For supersonic cases such as SBLI, a reconstruction limiter is required to suppress spurious oscillations near the shock. A smooth limiter tuned to the upwind-biased spatial differencing scheme was employed, as described in Krist et al. [6].

There are several turbulence models available in CFL3D. All are solved loosely-coupled to the Navier-Stokes equations. For the current SBLI applications, only the one-equation Spalart-Allmaras (SA) model [9] was employed. This turbulence model is widely used throughout the aerospace community for applications that include subsonic, transonic, and supersonic flows. It is also considered to be a good model for predicting both attached flows as well as flows with small regions of separation, including shock-induced separation. For all applications here, the model was active everywhere (fully turbulent flow was assumed).

3 The Experiments

There were four sets of experiments used for the workshop. One of these was conducted at the Institut Universitaire des Systemes Thermiques Industriels (IUSTI) in Marseille, France [10], in support of a European Union project titled UFAST [11]. The other three were conducted at the University of Michigan (UM) [12], as part of the U.S. Air Force sponsored Collaborative Center for the Aeronautical Sciences (CCAS). Two of the cases were open (experimental data were supplied to workshop participants ahead of time) and two were blind (no experimental data were available to participants). Some of the details regarding the four experiments are given in Table 1. For the IUSTI (UFAST) experiment the shock generator spanned the tunnel, whereas for the UM (CCAS) experiments it did not. Additional details can be found in DeBonis et al. [3] or on the workshop's website ¹. Particle Image Velocimetry (PIV) was used to obtain measurements of velocities as well as turbulence quantities in the interaction regions of the experiments. DeBonis et al. [3] also has a good discussion of the experimental uncertainties.

It is important to note that these SBLI cases are three-dimensional. This realization was one of the major outcomes of the UFAST project [4, 13]. Corner vortices in the tunnel test section affect the entire flow field, including the shock and interaction region in the center of the test section away from the corners. Therefore, computations must include the three-dimensional geometry, including all tunnel walls, in order to properly account for the flow physics. Some of the three-dimensional behavior of these cases will be shown in the Results section.

4 Results

Table 2 summarizes the computer runs performed using CFL3D. The fine grids for each case, consisting of between 7 and 9 million cells, were created at NASA Glenn Research Center by N. Georgiadis, M. Vyas, and D. Yoder for use by both the WIND code at NASA Glenn and the CFL3D code at NASA Langley. All grids assumed spanwise symmetry; i.e., one spanwise boundary was modeled as a solid wall, while the other spanwise boundary (the centerline plane) used a symmetry

¹<http://sbliworkshop.engin.umich.edu/html/>, cited 8/12/2010.

Table 2. Summary of CFL3D Cases Run

Case	Grid size (millions of cells)	flux scheme	thin vs. full
IUSTI (UFAST) $\theta = 8.0^\circ$	7.07	FVS	thin
	0.88	FVS	thin
	0.11	FVS	thin
UM (CCAS) $\theta = 7.75^\circ$	7.84	FVS	thin
	0.98	FVS	thin
	7.84	FDS	thin
	0.98	FDS	thin
	0.98	FDS	full
UM (CCAS) $\theta = 10.0^\circ$	8.50	FVS	thin
UM (CCAS) $\theta = 12.0^\circ$	8.50	FVS	thin

boundary condition. A limited number of grid convergence studies were performed for the IUSTI (UFAST) $\theta = 8.0^\circ$ and UM (CCAS) $\theta = 7.75^\circ$ cases, and the effect of flux scheme and thin-layer vs. full Navier-Stokes was briefly looked at for the UM (CCAS) $\theta = 7.75^\circ$ case. The results of these studies will be described in their respective sections below.

4.1 UFAST Case

An overall view of the UFAST fine grid is shown in Fig. 2. All distance units are in mm. This grid contained 10 zones, most of which were connected in a point-matched (one-to-one) fashion. There was one patched interface located between the two zones approximately 212 mm upstream of the leading edge of the shock generator. The shock generator itself had a blunt leading edge (not visible in the figure). The shock generator extended from approximately $x = 173$ mm to $x = 331$ mm, and spanned the tunnel. Each of the fine grid zones contained 81 points in the spanwise direction, with clustering along the tunnel side wall. The grids were designed to yield minimum spacings at walls with $y^+ \approx 1$ (approximately 0.005 mm). Near the edge of the incoming boundary layer, wall-normal spacing was $\Delta y \approx 1$ mm.

The flow conditions were: $M = 2.25$, $T_\infty = 145.590$ K, and $Re = 5684$ per mm. This Reynolds number was based on an assumed freestream density of $\rho_\infty = 0.1045$ kg/m³, speed of sound of $a_\infty = 241.85$ m/s, and viscosity of $\mu_\infty = 1.0004 \times 10^{-5}$ kg/(ms). Boundary conditions were as follows. All tunnel walls (top, bottom, and side) and the shock generator used no-slip adiabatic wall conditions. Symmetry was enforced along the centerplane. At the upstream boundary located at $x = -621$ mm, total conditions were specified as: $p_t/p_\infty = 11.56314$ and $T_t/T_\infty = 2.0125$. At the downstream boundary located at $x = 1000$ mm, all quantities were extrapolated from the interior of the domain.

The iterative convergence history of the density residual on the fine grid is shown in Fig. 3. It converged a little more than 3 orders of magnitude. The cause of the lack of global convergence beyond that point is not known. Sometimes the use of a reconstruction limiter causes convergence flattening like this, because of “flip-flopping” (sequentially turning on then off) of the limiter function in high gradient areas, e.g., near shock waves. It is also possible that the loss of convergence was in part caused by a very large region of separated flow located above and behind the shock generator. This separated region was far removed and downstream from the shock boundary layer interaction area of interest near the lower wall below the shock generator. The flow field in the area of interest did not change noticeably over the course of the final several thousand multigrid cycles.

A grid study was conducted for this case by running a fine, a medium, and a coarse level. Each level was constructed by removing every other grid point from the next finer grid. Results for u -velocity profiles and $-u'v'$ profiles at four stations near the interaction region are shown in Figs. 4

and 5. Overall, there was only a relatively small effect of the grid on u -velocity, but an exception to this was the region near the forward part of the separation zone ($x = 300 - 310$ mm). In this area there were larger changes in u -velocity due to grid refinement. The overall grid influence on $-u'v'$ was even more significant. In this case, the coarse grid was clearly too coarse to adequately represent this quantity. The results on the medium and fine grids were closer to each other, again with the largest difference near $x = 310$ mm. The peak $-u'v'$ changed by approximately 6% between the medium and fine levels at this location. While this is mostly a qualitative grid sensitivity analysis, it gives a feel for the discretization error influence on particular quantities of interest when using these grid sizes. It appears that – on the whole – the fine grid may be reasonable for obtaining engineering accuracy, but it is probably not fine enough to adequately resolve the region near the start of the separation bubble in the interaction region. It would be instructive to learn the influence of an extra-fine grid on this sensitive region.

Centerplane contours of CFD results on the fine grid are compared to experimental PIV data in Figs. 6 (a) – (c). The length of the separated region was approximately the same in both the CFD and the experiment, although the bubble height was predicted slightly smaller by the CFD. The magnitudes of the peak levels of $-u'v'$ were predicted too high by the CFD. However, overall there was fairly good correspondence between CFD and experiment in all quantities shown. Profiles at specific x -locations are given in Figs. 7, 8, and 9. The u -velocity profiles were predicted with higher magnitude than experiment downstream of $x = 300$ mm. The v -velocities overall were predicted reasonably well, except near $x = 320$, where the CFD missed the peak near $y = 9$ mm. This difference can also be seen in Fig. 6 (b), where the red contours of high v -velocity in the experiment can be seen to extend slightly higher and further downstream than in the CFD solution.

The three-dimensionality inherent in this case can be seen in the near-bottom wall streamlines, shown in Fig. 10. The CFD separated region showed similar features as experiment in the plane $y = 1$ mm above the bottom wall. The CFD bubble in that plane extended from an upstream extent near $x = 312$ mm, to a downstream extent near $x = 328$ mm, and lateral extent near $z = 45$ mm. In both CFD and experiment there was a curved reattachment line with maximum downstream extent at the centerplane.

4.2 CCAS Cases

An overall view of the UM fine grid (for $\theta = 7.75^\circ$) is shown in Fig. 11. All distance units are in mm. The grids for the other two CCAS shock angles were similar, so they will not be described in detail. However, Fig. 12 shows a comparison of the three shock generator shapes near their leading edges. Note that when the grids were created, a very small bluntness of a total height 0.06 mm was specified at the leading edges. The grid contained 16 zones, most of which were connected in a point-matched (one-to-one) fashion. There were two patched interfaces located at approximately $x = -92$ mm and at $x = 221$ mm. The $\theta = 7.75^\circ$ shock generator extended from approximately $x = -47$ mm to $x = 121$ mm, and spanned only the center region of the tunnel (between $z = -15.875$ to 15.875 mm when reflected across the center symmetry plane at $z = 0$). The shock generator was held in place from above by a narrow body located between $x = 0$ and approximately $x = 95$ mm. The tunnel side wall was located at $z = 28.575$ mm. The fine grid zones contained 141 points in the spanwise direction in the region of interest below the shock generator, with clustering along the tunnel side wall. The grids were designed to yield minimum spacings at walls with $y^+ \approx 1$ (approximately 0.005 mm). Near the edge of the incoming boundary layer, wall-normal spacing was $\Delta y \approx 1$ mm.

The flow conditions were: $M = 2.75$, $T_\infty = 116.617$ K, and $Re = 8831$ per mm. This Reynolds number was based on an assumed freestream density of $\rho_\infty = 0.120$ kg/m³, speed of sound of $a_\infty = 216.4$ m/s, and viscosity of $\mu_\infty = 8.0863 \times 10^{-6}$ kg/(ms). Boundary conditions were as follows. All tunnel walls (top, bottom, and side) and the shock generator used no-slip adiabatic wall conditions. Symmetry was enforced along the centerplane. At the upstream boundary located at $x = -949$ mm, total conditions were specified as: $p_t/p_\infty = 25.14207$ and $T_t/T_\infty = 2.51251$. At the downstream boundary located near $x = 600$ mm, all quantities were extrapolated

from the interior of the domain.

The global iterative convergence behaviors of the UM cases were worse than the UFAST case. The reason for lack of overall convergence over the entire field is not known. However, like the UFAST case, the UM cases were run long enough until the flow in the SBLI area of interest near the bottom wall did not change appreciably.

A grid convergence study was performed using two successive grids for the $\theta = 7.75^\circ$ case. The u -velocity profiles and $-u'v'$ profiles at four locations along the centerplane in the interaction region are shown in Figs. 13 and 14. Overall, the effect of grid (between 0.98 million cells and 7.84 million cells) on u -velocity was relatively small, with the largest influence occurring near the beginning of the interaction region, at $x = 30$ mm. On the other hand, the effect on $-u'v'$ was more significant, particularly at the $x = 35$ mm station. Here, the peak level nearest the wall varied by over 13%, and a second peak near $y = 5$ mm was missed by the coarser grid (this double peak in $-u'v'$ occurred underneath the beginning of the reflected shock; there was a similar double peak evident in the UFAST experimental data shown in Fig. 9 at $x = 320$ mm). At other locations, the coarser grid underpredicted the peak by as much as about 10%. Thus, the fine grid with 7.84 million cells may be reasonable for obtaining engineering accuracy in u -velocity, but it is not clear how accurate it is for turbulence quantities. A finer grid would be required to answer this question. Although not readily discernible in Fig. 13, it should be noted that there was no separated flow predicted along the centerplane on the medium grid, but a small, very thin region of reverse flow was predicted along the centerplane on the fine grid between $x = 29$ and 36.5 mm.

Fig. 15 shows the effect of using FDS (as opposed to FVS) on u -velocities for this case, as well as the effect of full Navier-Stokes (as opposed to thin-layer, with viscous derivatives in all coordinate directions but no cross-derivative terms). Only the coarser grid with 0.98 million cells was used for the results in this figure. FDS had a tendency to yield higher velocity at a given distance from the wall than FVS, particularly at $x = 30$ mm. There was very little difference evident between thin-layer and full Navier-Stokes results on the centerplane in the interaction region. Focusing on the sensitive $x = 30$ mm location, the effect of grid density on both FVS and FDS is shown in Fig. 16. For both schemes, refining the grid caused higher velocity levels (“fuller” profiles) at this location. Although not shown, there was less grid influence at other stations.

Bottom wall surface-restricted streamlines are shown in Fig. 17. All three methods (FVS thin-layer, FDS thin-layer, and FDS full) produced very similar results, including the size and shape of the large sidewall interaction region. The main noticeable difference was near the centerplane, where the full Navier-Stokes result yielded a very small region of reverse flow, and the others did not.

Contours of CFD results on the fine grid are compared to preliminary experimental PIV data in Figs. 18(a) – (b). The PIV grid points (onto which the CFD data were interpolated for the workshop) were not close enough to the wall to include any of the very small, thin separated region predicted by CFD on the fine grid in this case. Note that there were large inconsistencies in some of the experimental data given at the workshop, at the intersections of the spanwise planes with the center streamwise plane. These inconsistencies were as large as 25 – 35%, and were also noted by DeBonis et al. [3], who chose to use only the centerplane measurements for comparisons. Also note that at the workshop, some concerns were raised regarding the preliminary experimental turbulence data released to the workshop participants. Therefore, no turbulence comparisons will be made here. Centerplane CFD comparisons of u -velocity and v -velocity are shown in Figs. 19 and 20. Predictions were fairly good for u -velocity, but were less accurate for v -velocity, although the same trends as experiment were exhibited.

Although not shown, the UM experimental data also included many derivative quantities such as $\partial u/\partial x$, $\partial u/\partial y$, $\partial u/\partial z$, etc. However, it is important to note that the PIV grid was used to find these derivatives in the experiment. Very near the surface, certain derivatives (such as $\partial u/\partial y$) had very large gradients – on the order of hundreds of thousands – and they changed rapidly in y . The PIV grid density in the y -direction (approximately 0.5 mm) was *not* fine enough to accurately determine this particular derivative in the high gradient regions.

The blind UM cases $\theta = 10^\circ$ and $\theta = 12^\circ$ were also computed on their respective fine grids. Because no experimental data were available for these cases at the time of the workshop, detailed results are not given here. However, general CFD-only comparisons between the three UM cases are shown in Figs. 21 – 23. The main influence of increasing shock angle was a slightly larger region of lower u -velocity flow in the interaction region on the centerplane. As seen in Fig. 23, all cases predicted regions of separated flow near the centerplane, but these regions were very thin so they did not show up when the CFD data was interpolated onto the PIV centerplane grids (whose closest approach to the wall was around 0.25 mm). The centerplane region was significantly affected by very strong sidewall interactions, which were larger for the higher shock angles.

5 Conclusions

Numerical simulations of four SBLI cases from the AIAA Supersonic Shock Boundary Layer Interaction Workshop were presented, using the compressible Reynolds-averaged Navier-Stokes CFD code CFL3D. The one-equation Spalart-Allmaras turbulence model was employed for all cases.

Grid convergence studies were conducted for two of the cases. Also, the effect of two different flux schemes and the effect of thin-layer vs. full Navier-Stokes was examined. The fine grids (between 7 and 9 million cells) were generally dense enough to yield reasonably grid-converged mean flow results over much of the interaction region, although the forward part of the interaction region on the centerplane was not grid-converged. Turbulence quantities were more grid-sensitive than the mean flow overall. Thus, finer grid levels than the ones used for the workshop would be necessary to more confidently assess the effects of discretization errors. Flux difference splitting was shown to yield somewhat higher velocity levels (“fuller” profiles) than flux vector splitting. The difference between thin-layer and full Navier-Stokes on the centerplane in the interaction region was very small in the case examined.

For the UFAST case, CFD predicted centerplane results in the interaction region reasonably well compared to experiment, with the exception that the velocity was predicted somewhat too full and the peak turbulence levels tended to be overpredicted in magnitude in the region where separated flow occurred. For the UM $\theta = 7.75^\circ$ case, u -velocity comparisons with experiment were overall fairly good. The computed v -velocity components exhibited the same trends as experiment, but were offset. Comparisons between CFD and experimental $-u'v'$ were not made for the UM case because of questions raised during the workshop regarding the latter preliminary data. Strong three-dimensional behaviors in and near the interaction regions were documented for all four SBLI cases.

References

1. Knight, D., “Numerical Simulation of 3-D Shock Wave Turbulent Boundary Layer Interactions,” *Special Course on Shock-Wave/Boundary Layer Interactions in Supersonic and Hypersonic Flows*, edited by G. Degrez, AGARD Rept. 792, 1993, pp. 3-1 – 3-32.
2. Benek, J. A., “Overview of the 2010 AIAA Shock Boundary Layer Interaction Prediction Workshop,” AIAA Paper 2010-4821, June-July 2010.
3. DeBonis, J. R., Oberkampf, W. L., Wolf, R. T., Orkwis, P. D., Turner, M. G., and Babinsky, H., “Assessment of CFD Models for Shock Boundary-Layer Interaction,” AIAA Paper 2010-4823, June-July 2010.
4. Hirsch, C., “Lessons Learned from the First AIAA-SWBLI Workshop CFD Simulation of Two Test Cases,” AIAA Paper 2010-4824, June-July 2010.
5. Benek, J. A., “Lessons Learned from the 2010 AIAA Shock Boundary Layer Interaction Prediction Workshop,” AIAA Paper 2010-4825, June-July 2010.
6. Krist, S. L., Biedron, R. T., and Rumsey, C. L., “CFL3D User’s Manual (Version 5.0),” NASA TM-1998-208444, June 1998.
7. Anderson, W. K., Thomas, J. L., and Van Leer, B., “Comparison of Finite Volume flux Vector Splittings for the Euler Equations,” *AIAA Journal*, Vol. 24, No. 9, 1986, pp. 1453–1460.
8. Roe, P. L., “Approximate Riemann Solvers, Parameter Vectors, and Difference Schemes,” *Journal of Computational Physics*, Vol. 43, 1981, pp. 357–372.
9. Spalart, P. R., and Allmaras, S. R., “A One-Equation Turbulence Model for Aerodynamic Flows,” *Recherche Aerospaciale*, No. 1, 1994, pp. 5–21.
10. Dupont, P., Piponnier, S., Sidorenko, A., and Debieve, J., “Investigation by Particle Image Velocimetry Measurements of Oblique Shock Reflection with Separation,” *AIAA Journal*, Vol. 46, No. 6, 2008, pp. 1365–1370.
11. Doerffer, P., “European Research on Unsteady Effects of Shock Wave Induced Separation UFAST-Project,” Paper ISAI8-0051, Proceedings of the 8th International Symposium on Experimental and Computational Aerothermodynamics of Internal Flows, Lyon, France, July 2007.
12. Lapsa, A. P. and Dahm, W. J. A., “Stereo Particle Image Velocimetry of Nonequilibrium Turbulence Relaxation in a Supersonic Boundary Layer,” *Experiments in Fluids*, 2010, online June 4, 2010.
13. Doerffer, P., Hirsch, C., Dussauge, J.-P., Babinsky, H., and Barakos, G.N. (Eds.), Unsteady Effects of Shock Wave Induced Separation, *Notes on Numerical Fluid Mechanics and Multidisciplinary Design*, Springer, 2010, ISBN 978-3-642-03003-1.

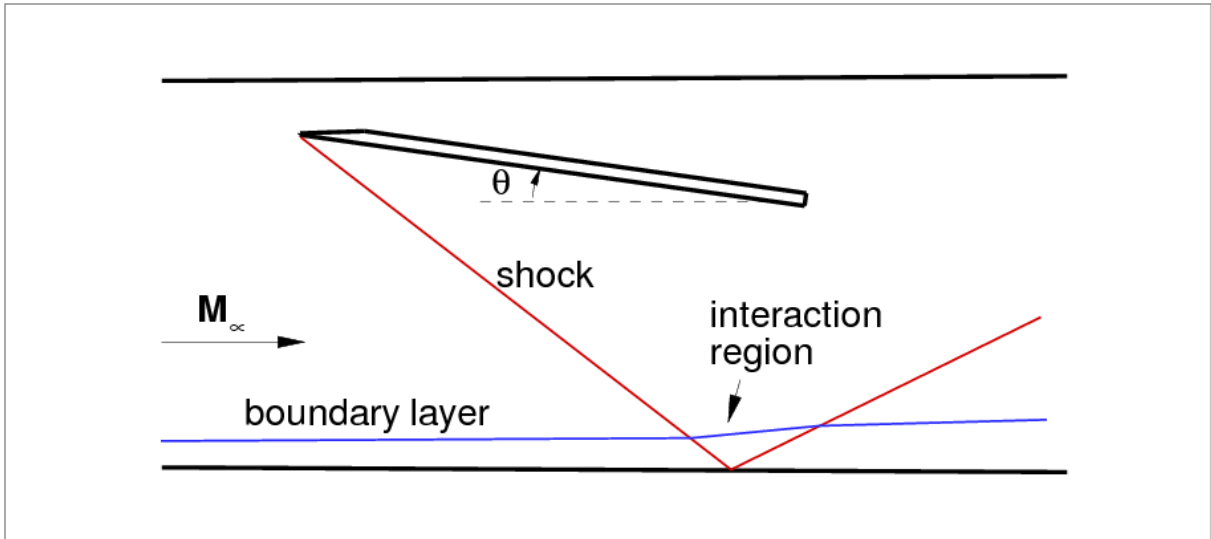
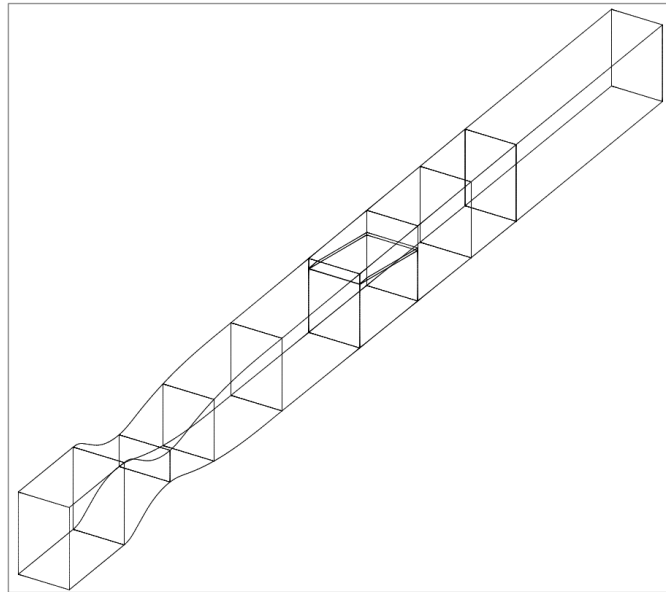
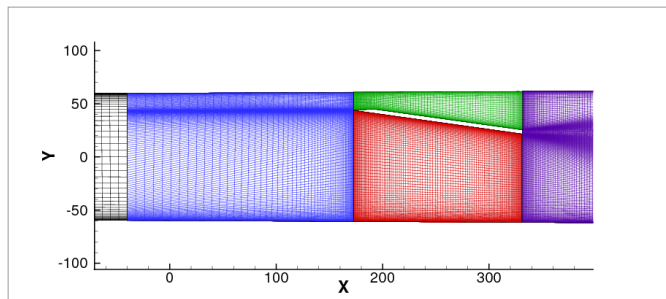


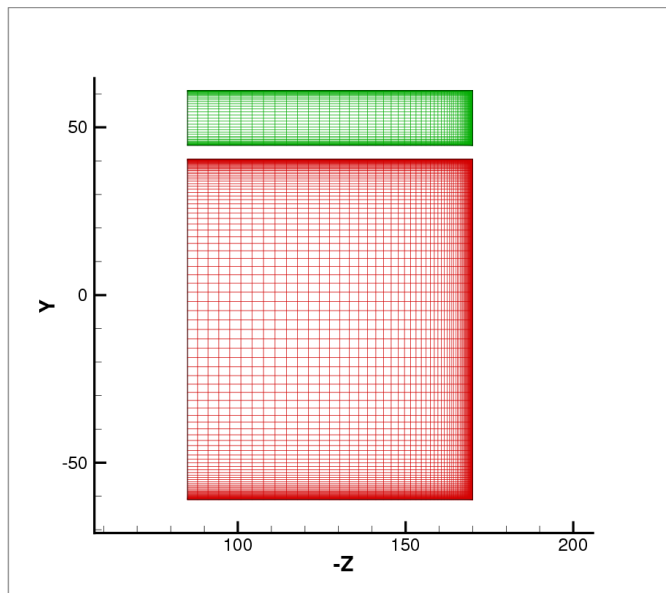
Figure 1. Schematic diagram of a SBLI.



(a) zone set-up, showing half-span configuration



(b) along symmetry plane near shock generator



(c) near $x = 190$ (centerline symmetry plane on left, side wall on right)

Figure 2. Views of UFAST fine grid.

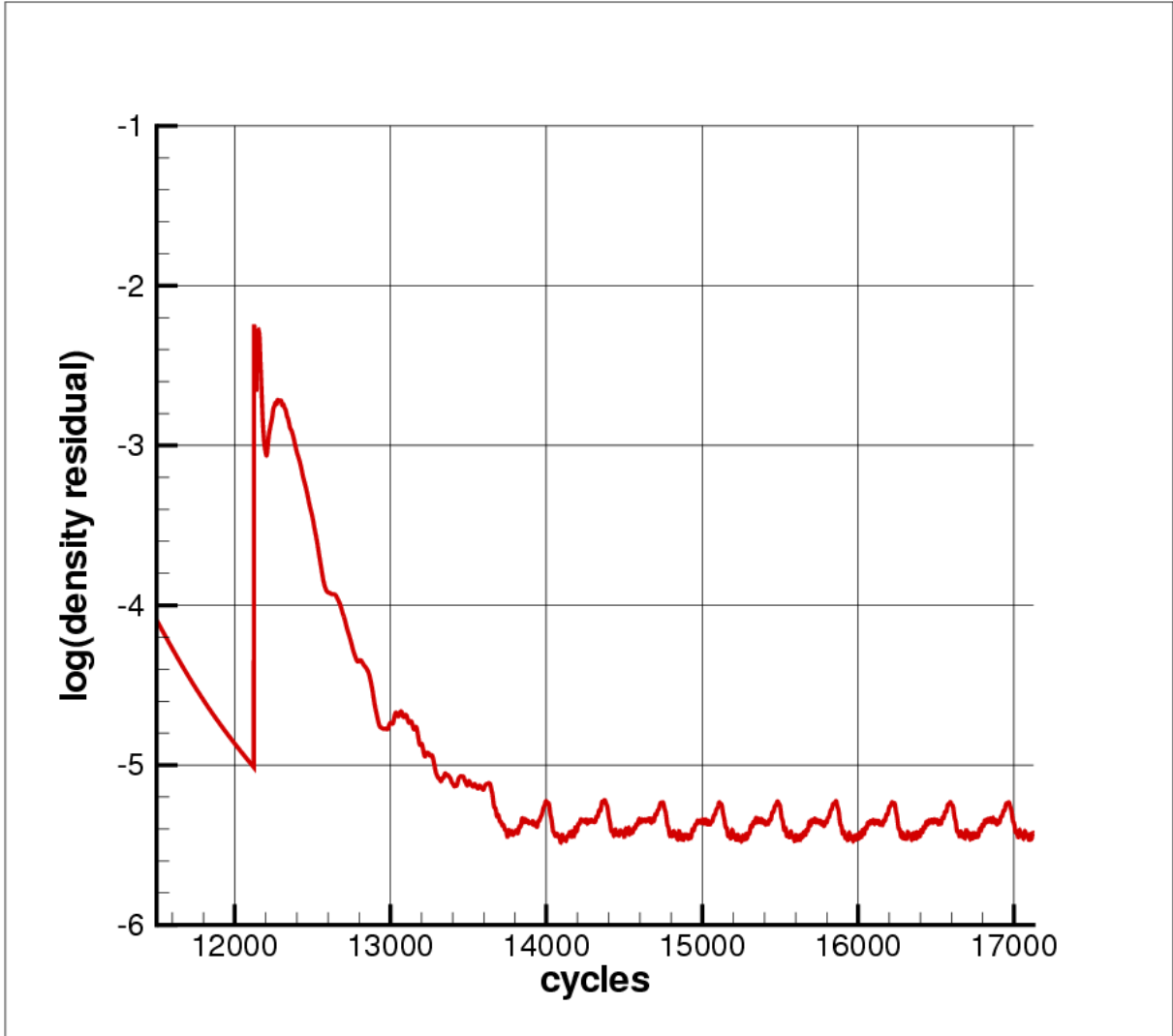


Figure 3. Convergence residual history for UFAST fine grid.

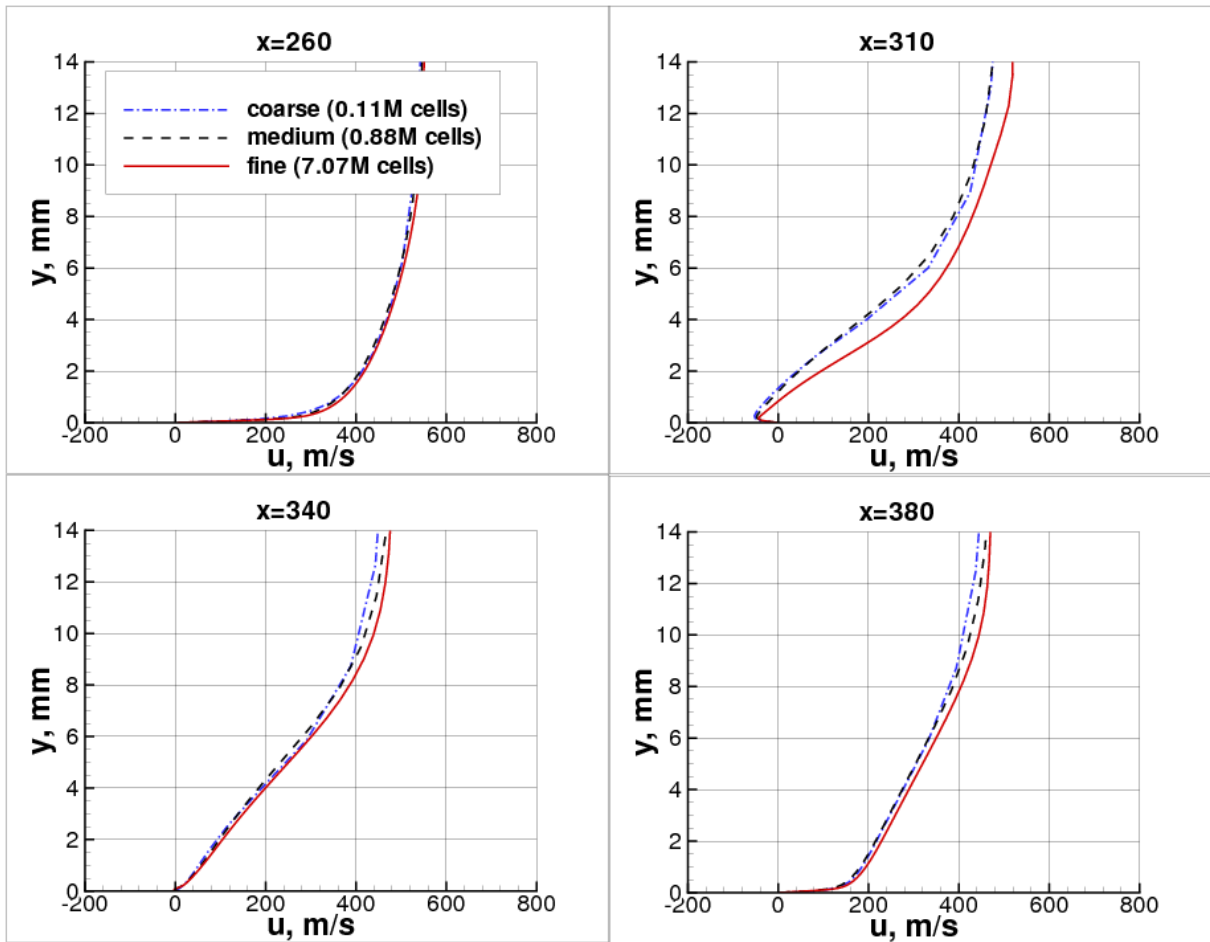


Figure 4. Grid effect on u -velocity profiles on the centerplane in the interaction region of the UFAST case.

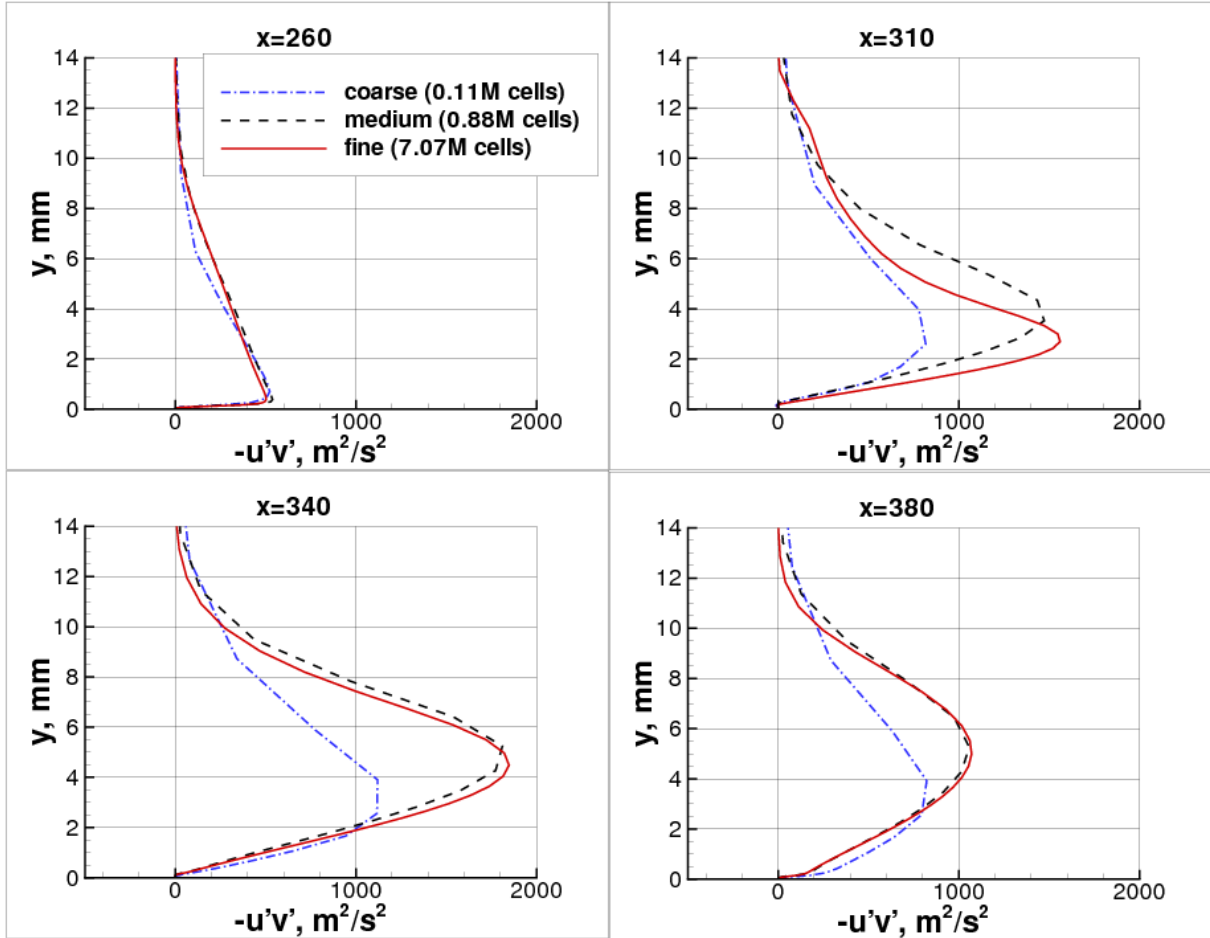


Figure 5. Grid effect on $-u'v'$ profiles on the centerplane in the interaction region of the UFAST case.

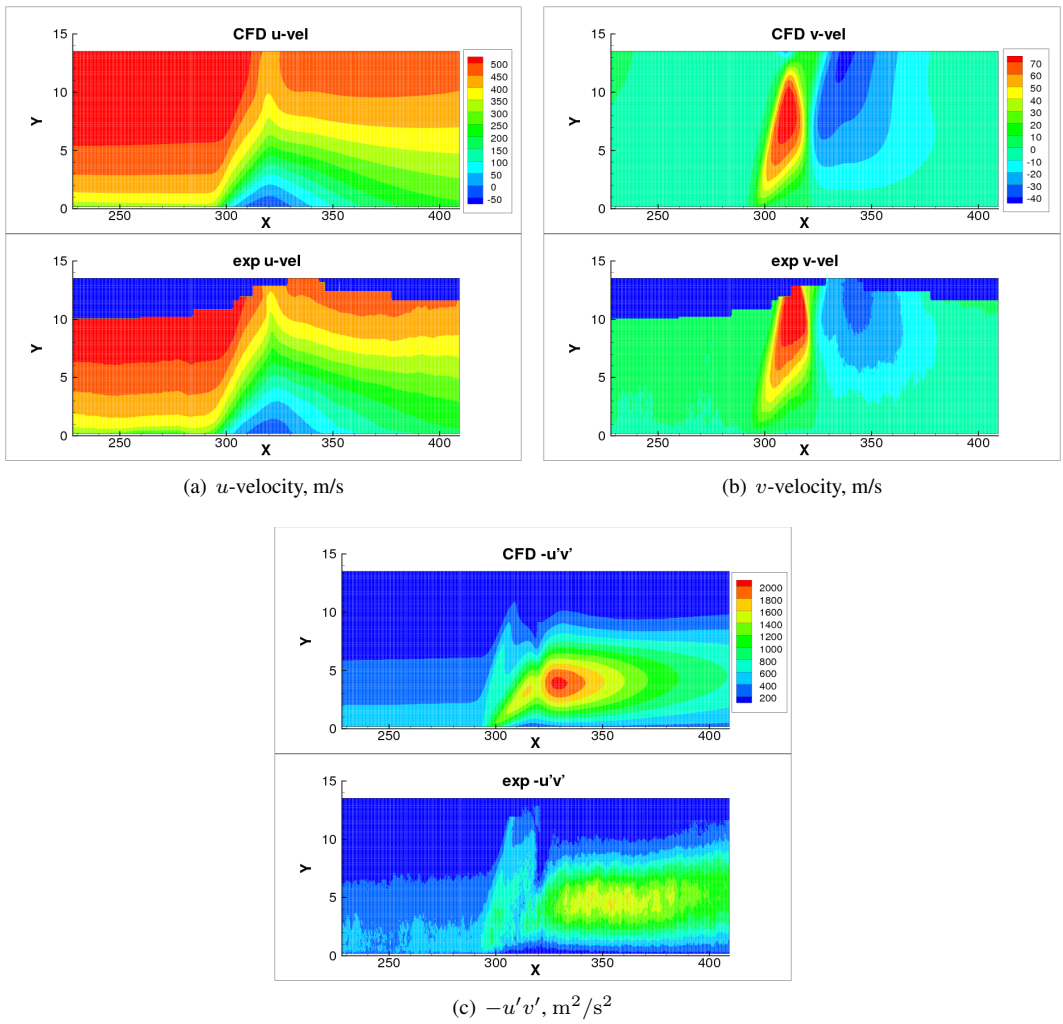


Figure 6. Centerplane contours for UFAST case (CFD results from fine grid have been interpolated to PIV grid points).

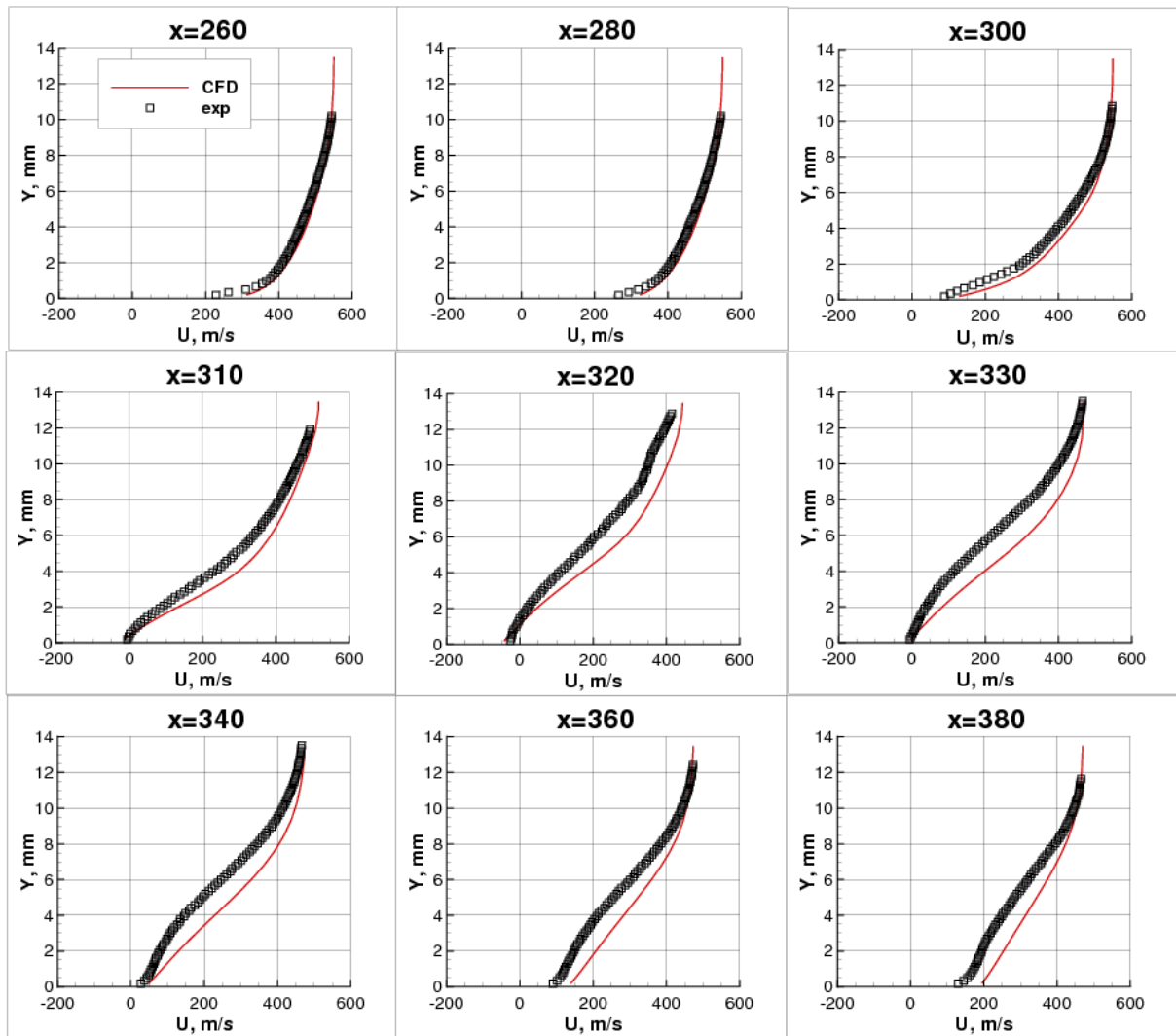


Figure 7. Centerplane u -velocity profiles for UFAST case (CFD results from fine grid have been interpolated to PIV grid points).

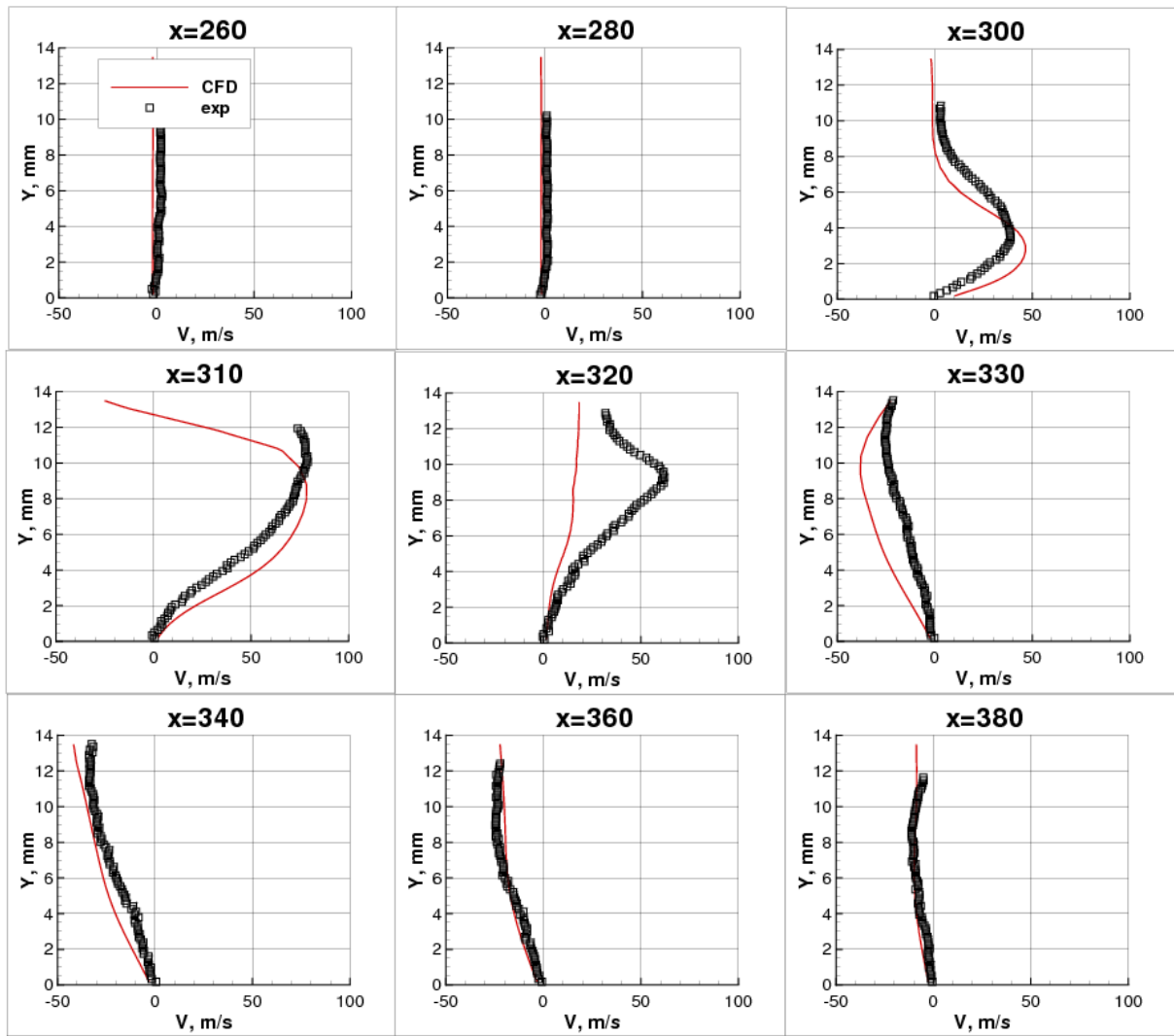


Figure 8. Centerplane v -velocity profiles for UFAST case (CFD results from fine grid have been interpolated to PIV grid points).

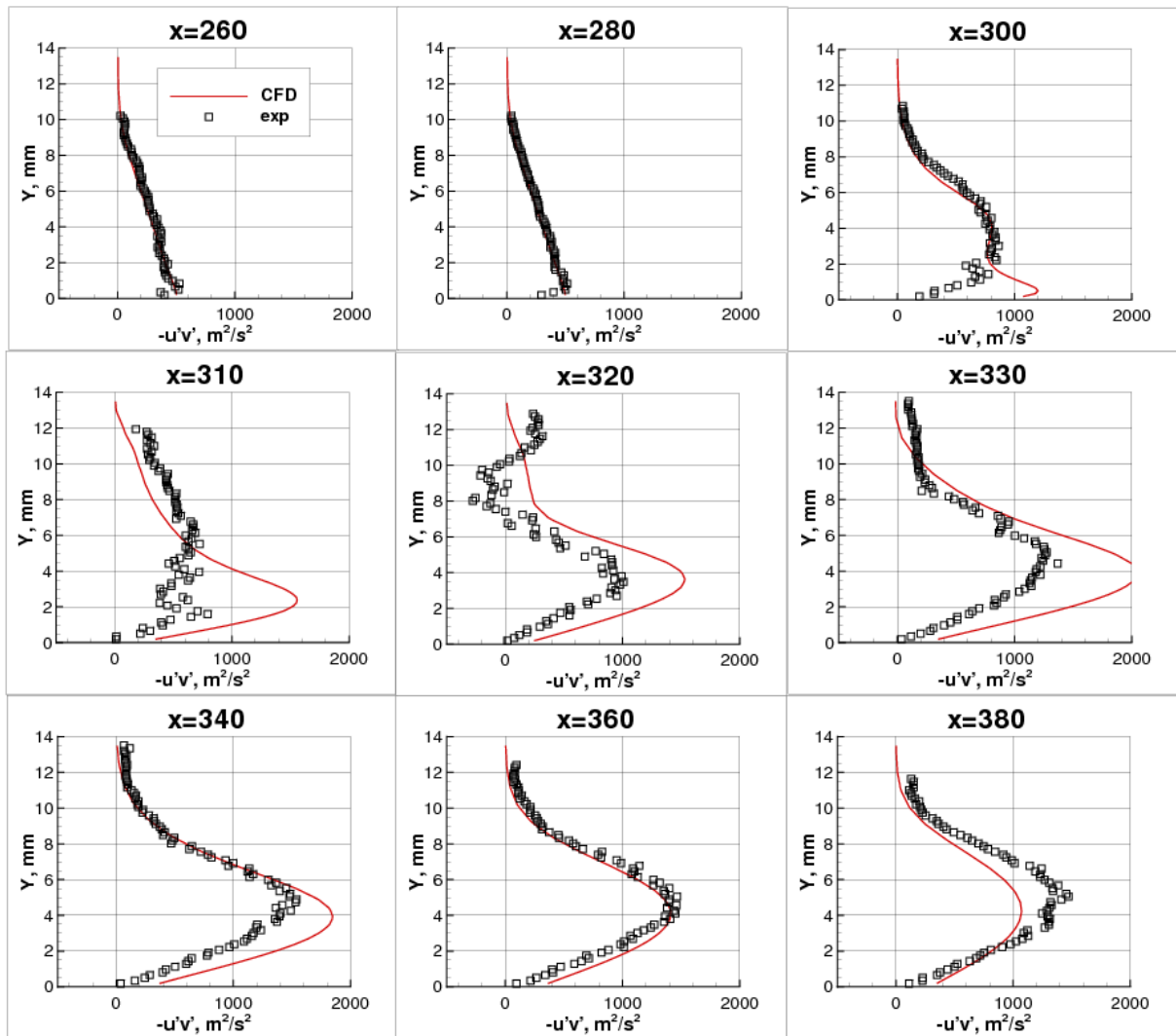
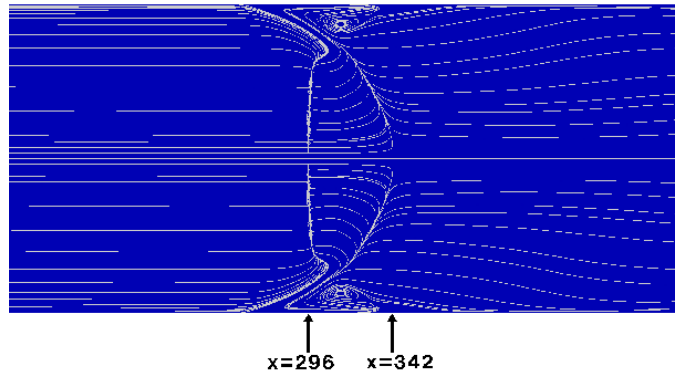
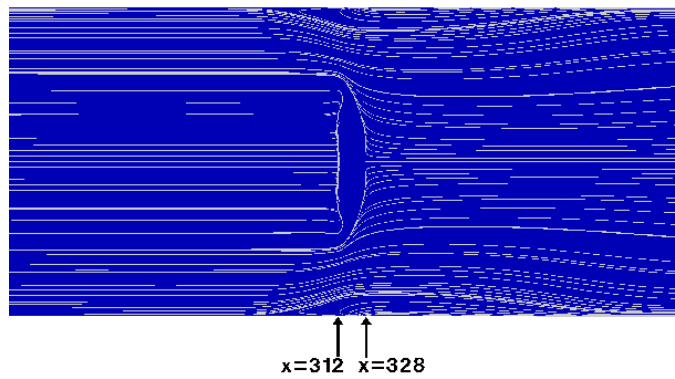


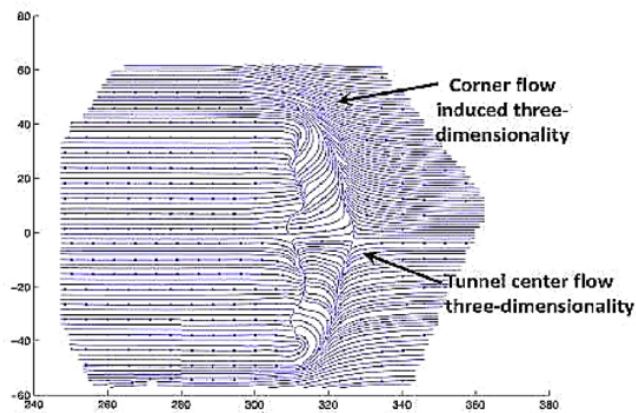
Figure 9. Centerplane $-u'v'$ profiles for UFAST case (CFD results from fine grid have been interpolated to PIV grid points).



(a) CFD bottom wall surface-restricted streamlines, with centerline separation extent denoted by arrows

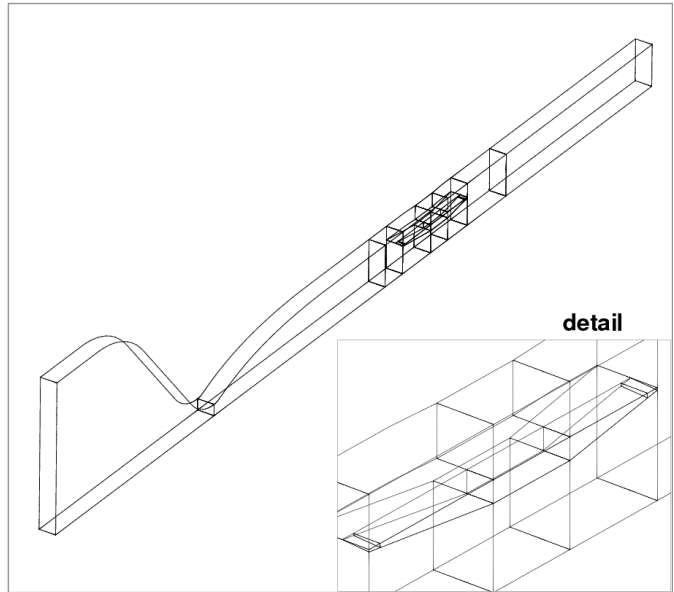


(b) CFD near $y = 1$ mm, with centerline separation extent denoted by arrows

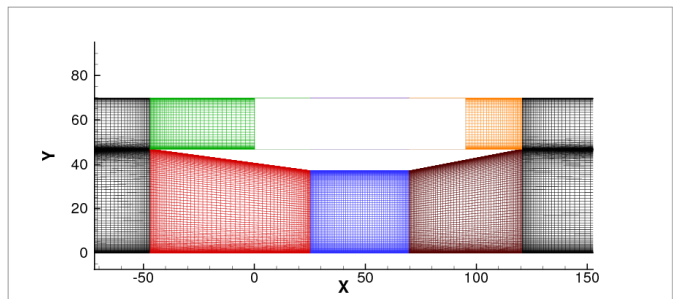


(c) IUSTI experiment near $y = 1$ mm, from Benek [2]

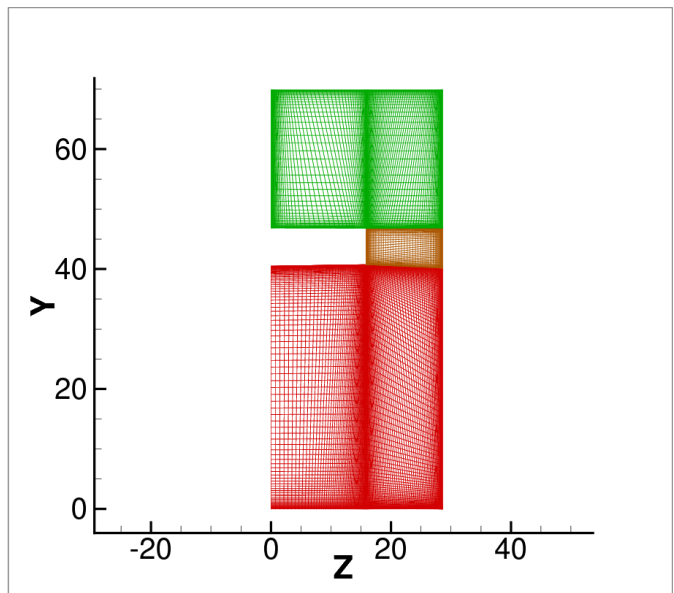
Figure 10. Streamlines at and near bottom wall in the interaction region for UFAST case (flow is from left to right).



(a) zone set-up, showing half-span configuration



(b) along symmetry plane near shock generator



(c) near $x = 0$ (centerline symmetry plane on left, side wall on right)

Figure 11. Views of UM $\theta = 7.75^\circ$ fine grid.

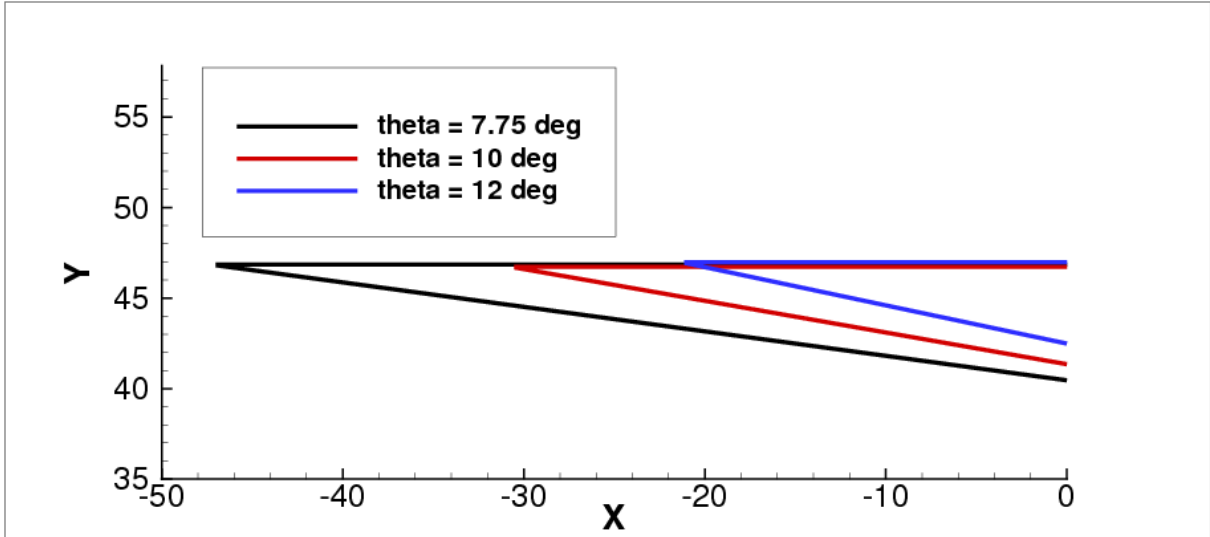


Figure 12. Comparison of shock generator shapes for the three different UM cases.

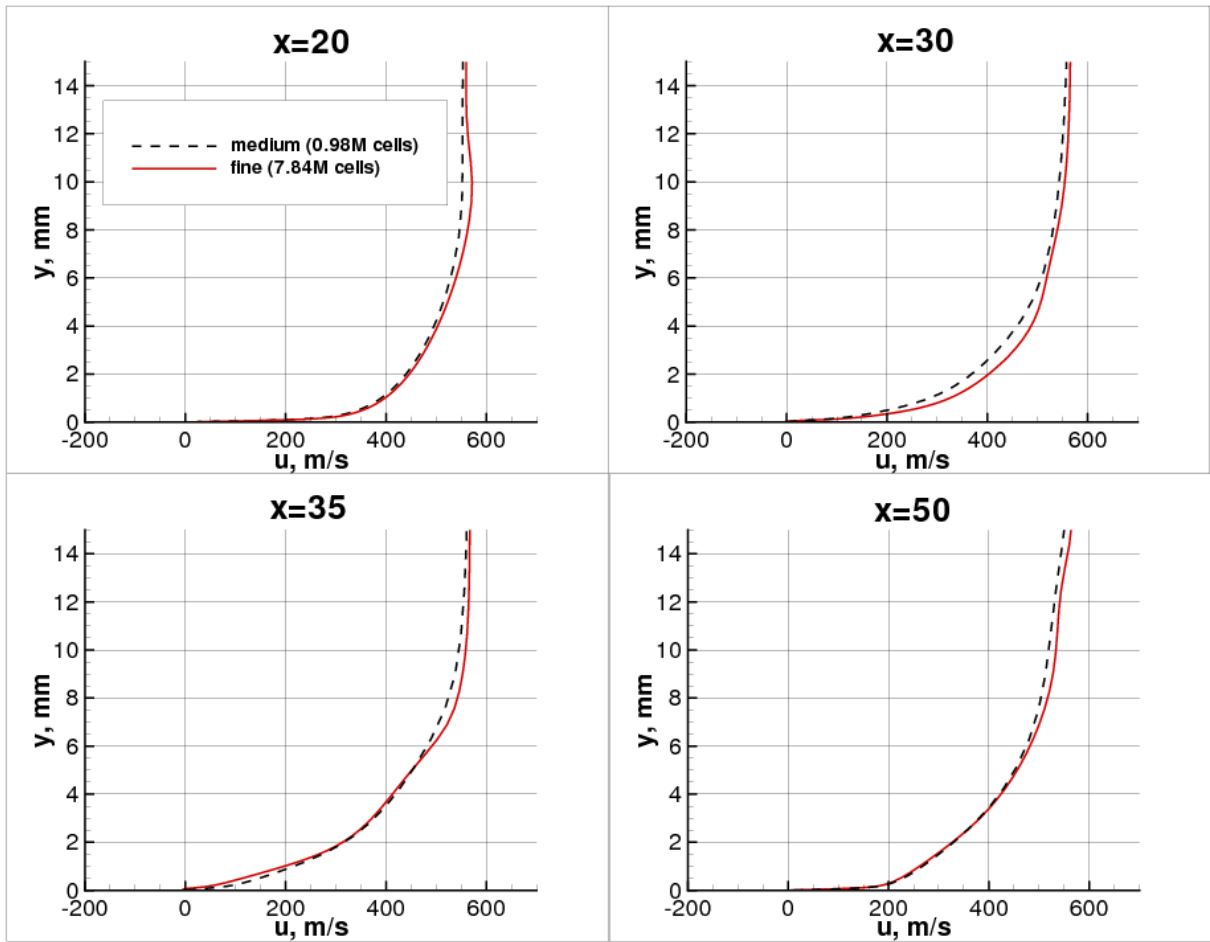


Figure 13. Grid effect on u -velocity profiles on the centerplane in the interaction region of the CCAS $\theta = 7.75^\circ$ case.

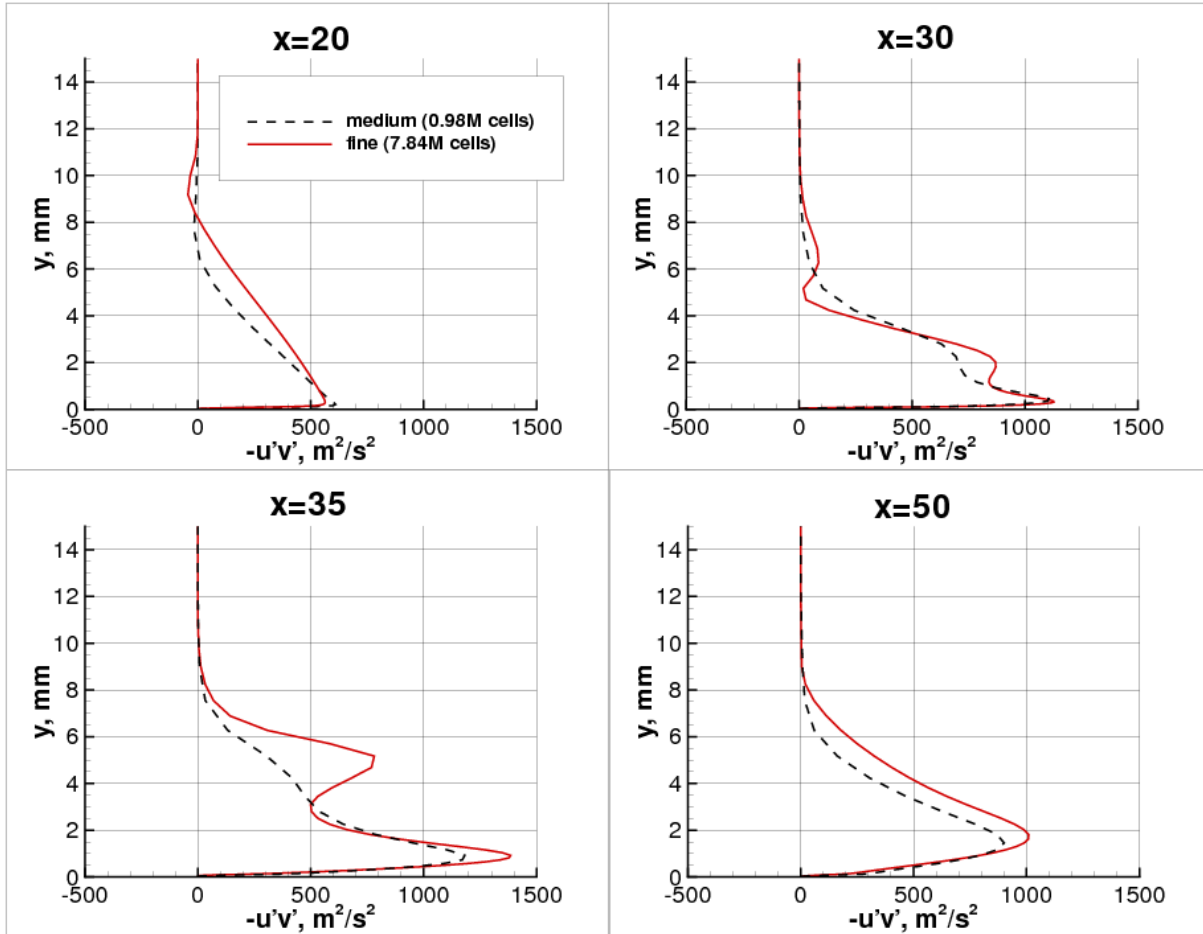


Figure 14. Grid effect on $-u'v'$ profiles on the centerplane in the interaction region of the CCAS $\theta = 7.75^\circ$ case.

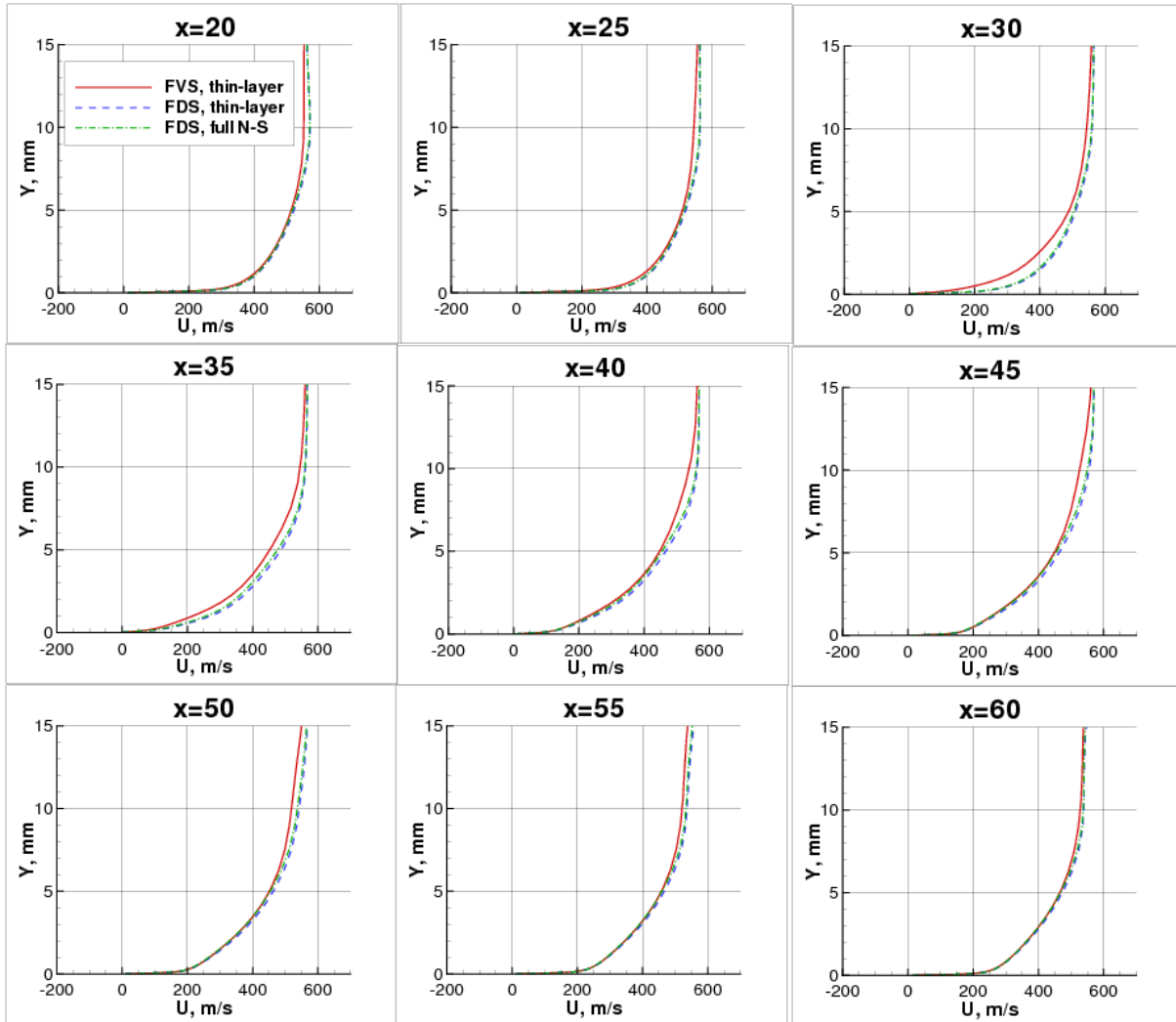


Figure 15. Effect of FDS and full Navier-Stokes on u -velocity centerplane profiles in the interaction region of the CCAS $\theta = 7.75^\circ$ case, 0.98 million-cell grid.

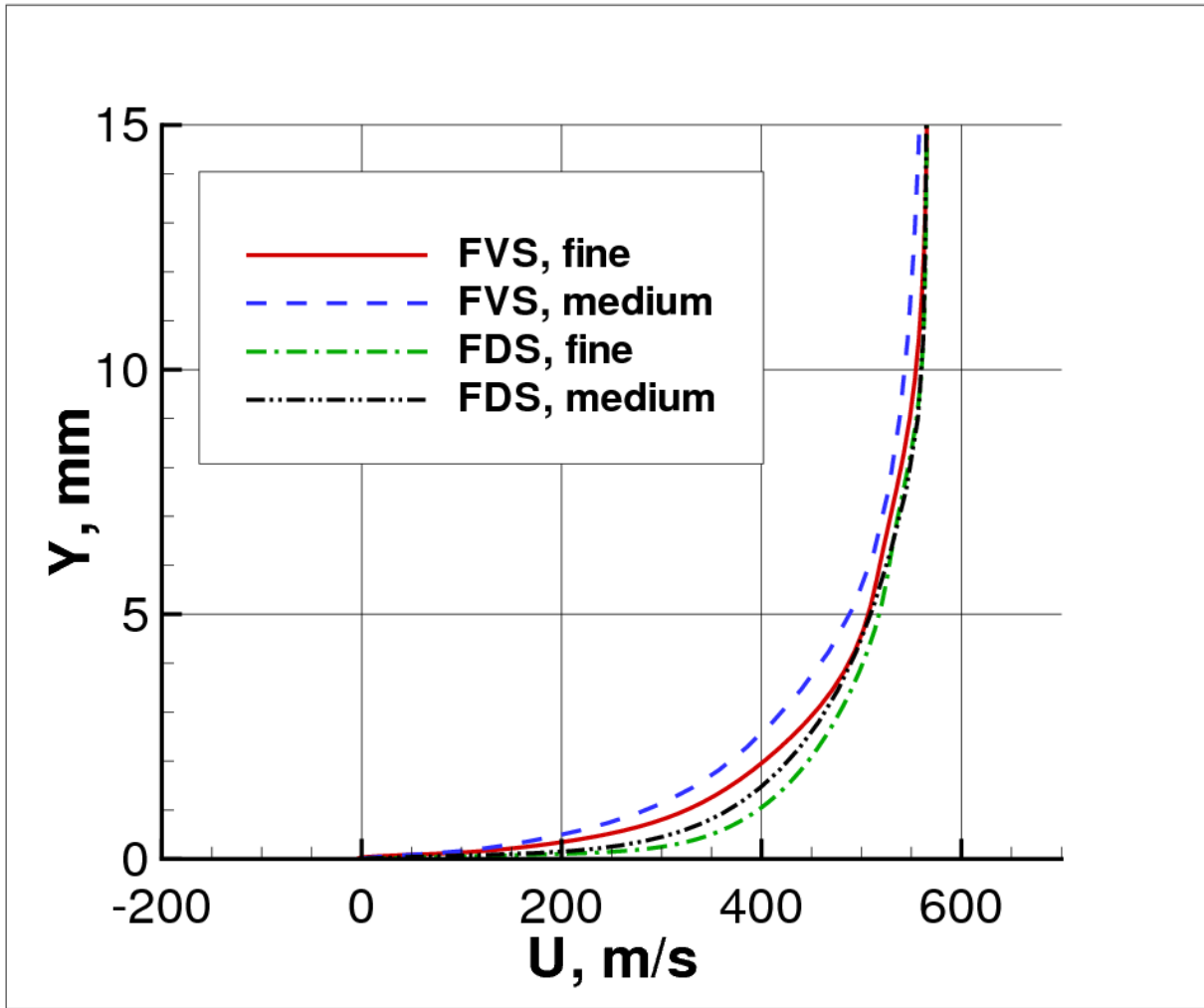
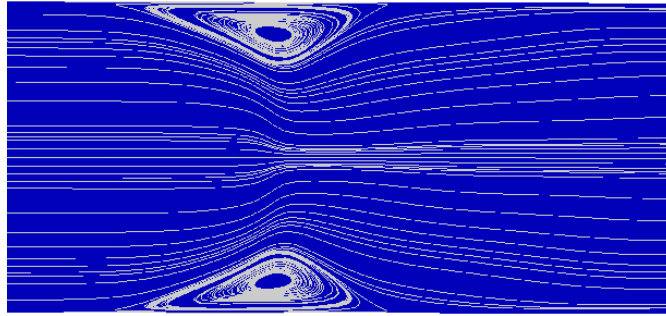
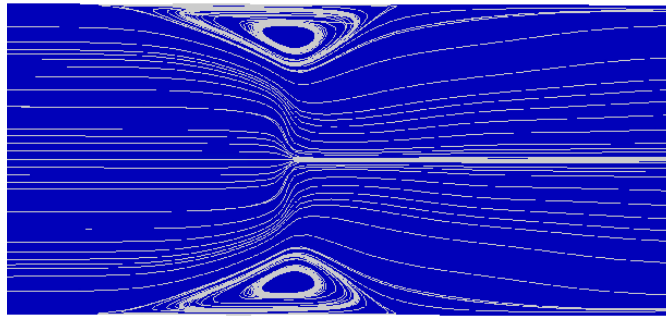


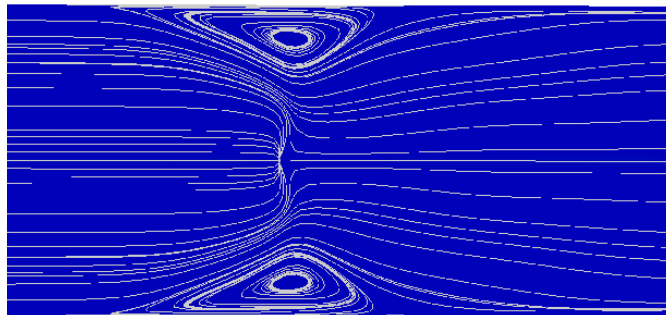
Figure 16. Grid effect on u -velocity profiles on the centerplane at $x = 30$ mm for FVS and FDS, CCAS $\theta = 7.75^\circ$ case.



(a) FVS, thin-layer Navier-Stokes

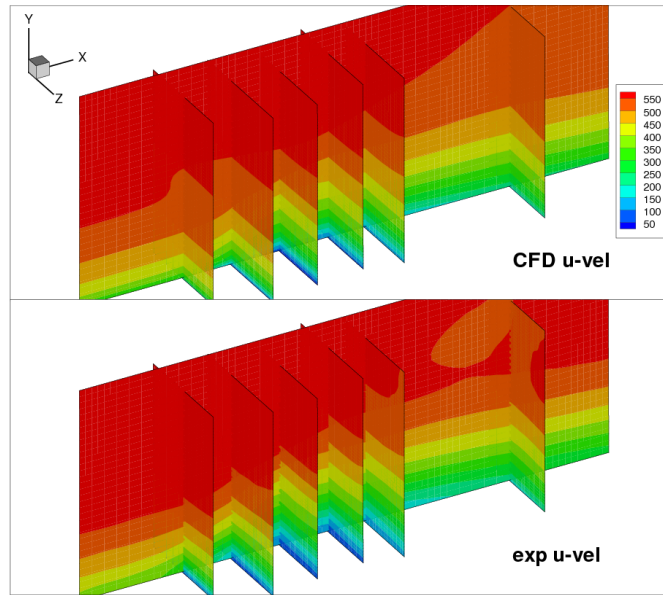


(b) FDS, thin-layer Navier-Stokes

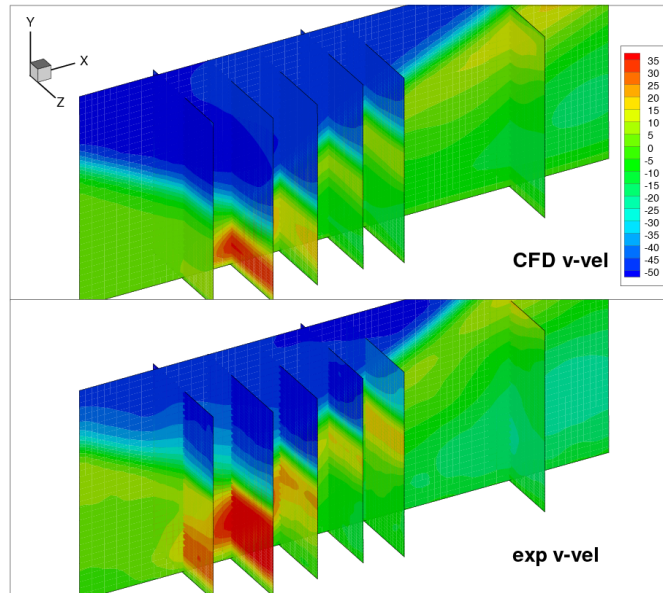


(c) FDS, full Navier-Stokes

Figure 17. CFD bottom wall surface-restricted streamlines in the interaction region for the CCAS $\theta = 7.75^\circ$ case, 0.98 million-cell grid (flow is from left to right).



(a) u -velocity, m/s



(b) v -velocity, m/s

Figure 18. Contours for CCAS $\theta = 7.75^\circ$ case (CFD results from fine grid have been interpolated to PIV grid points).

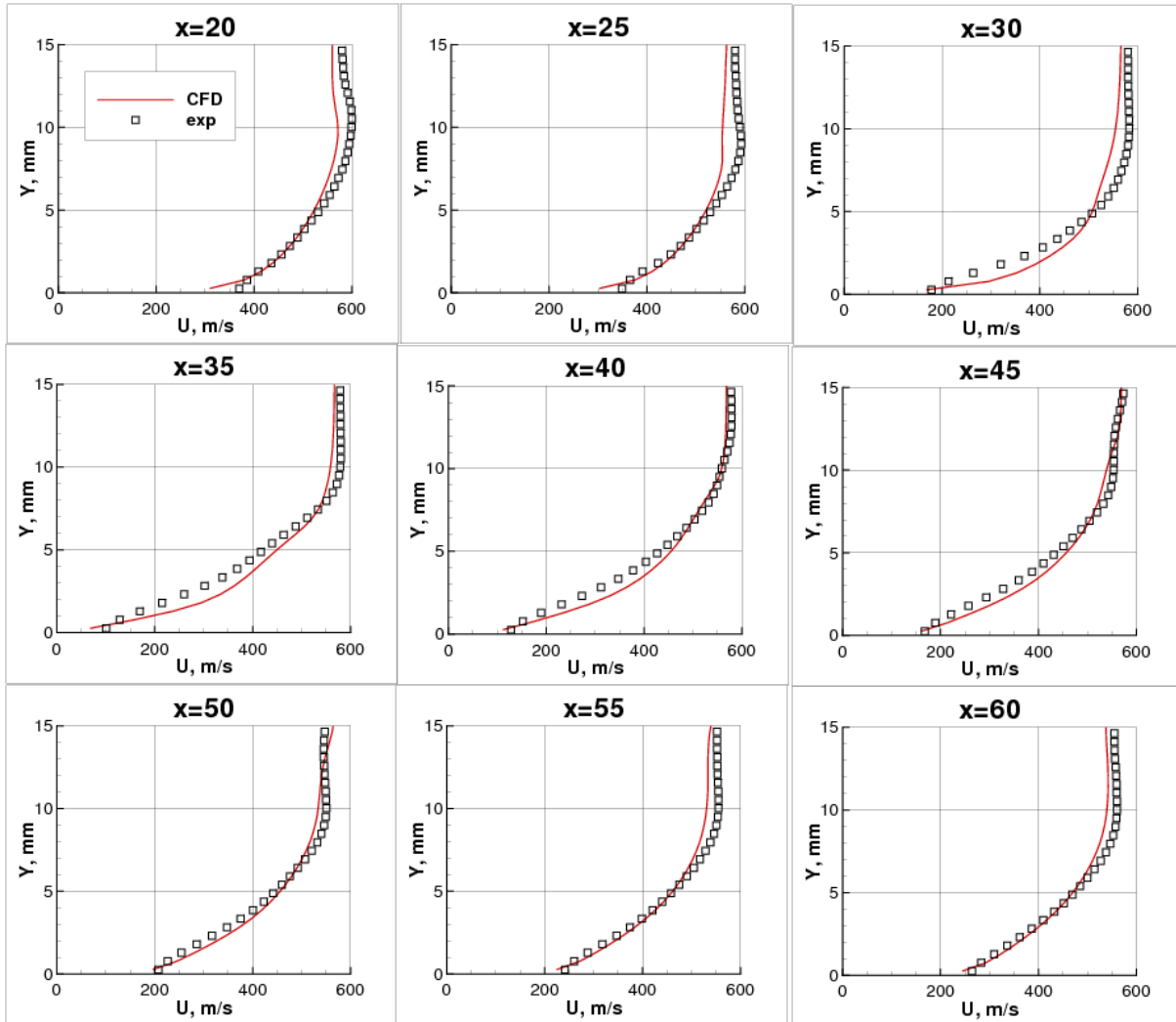


Figure 19. Centerplane u -velocity profiles for CCAS $\theta = 7.75^\circ$ case (CFD results from fine grid have been interpolated to PIV grid points).

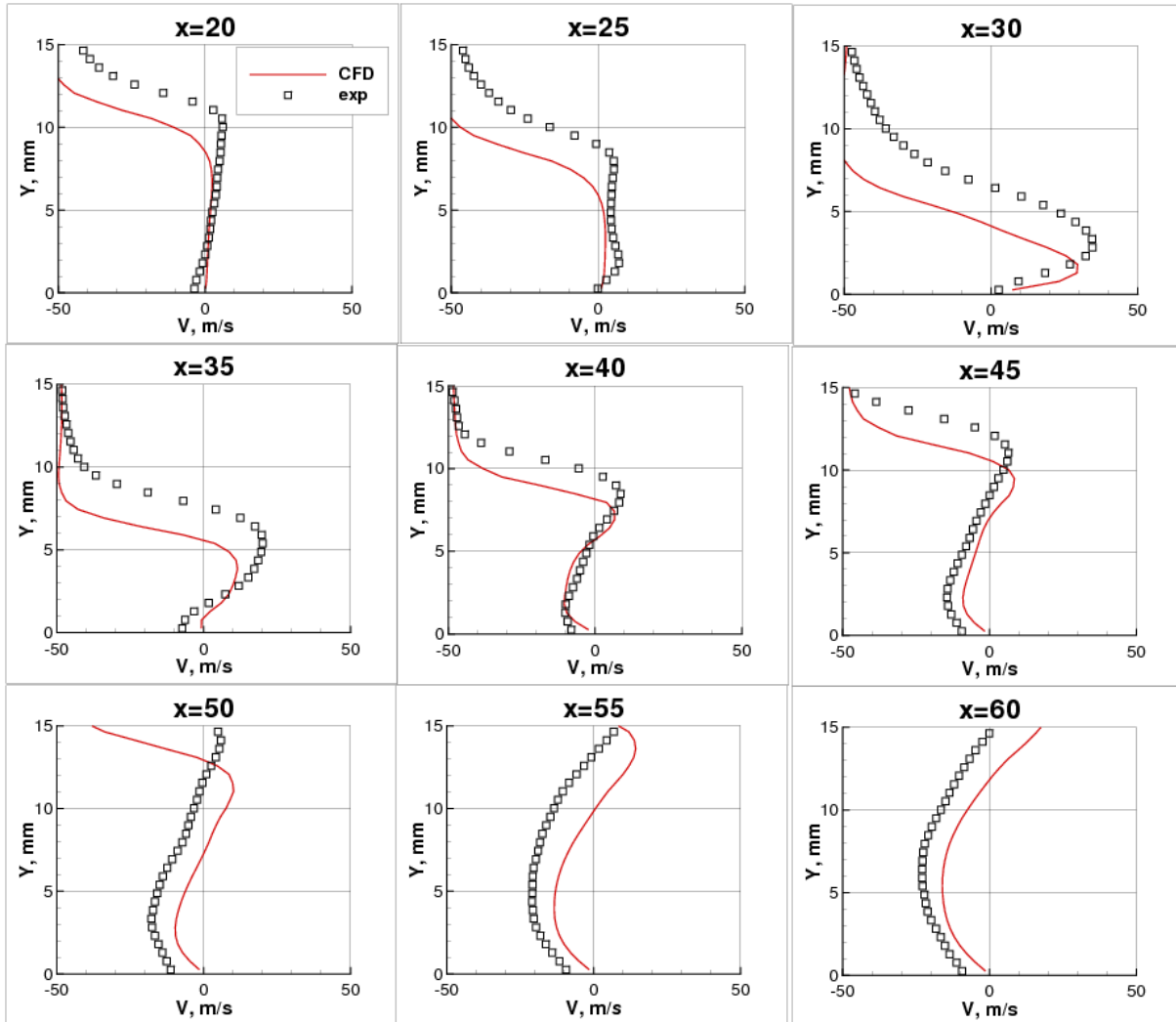


Figure 20. Centerplane v -velocity profiles for CCAS $\theta = 7.75^\circ$ case (CFD results from fine grid have been interpolated to PIV grid points).

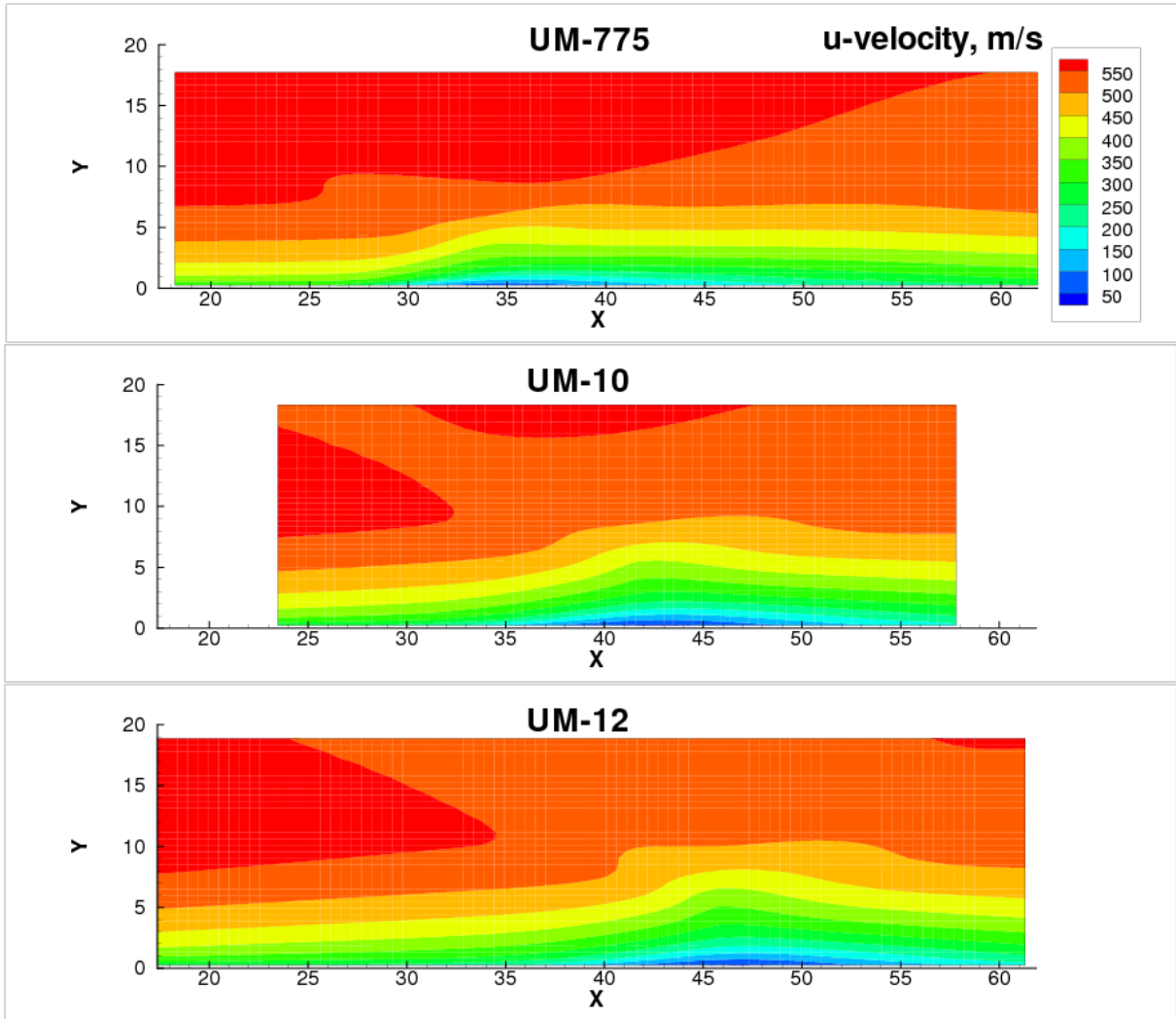


Figure 21. Comparison of centerplane CFD fine-grid u -velocity contours for all three CCAS cases (CFD results from fine grid have been interpolated to PIV grid points).

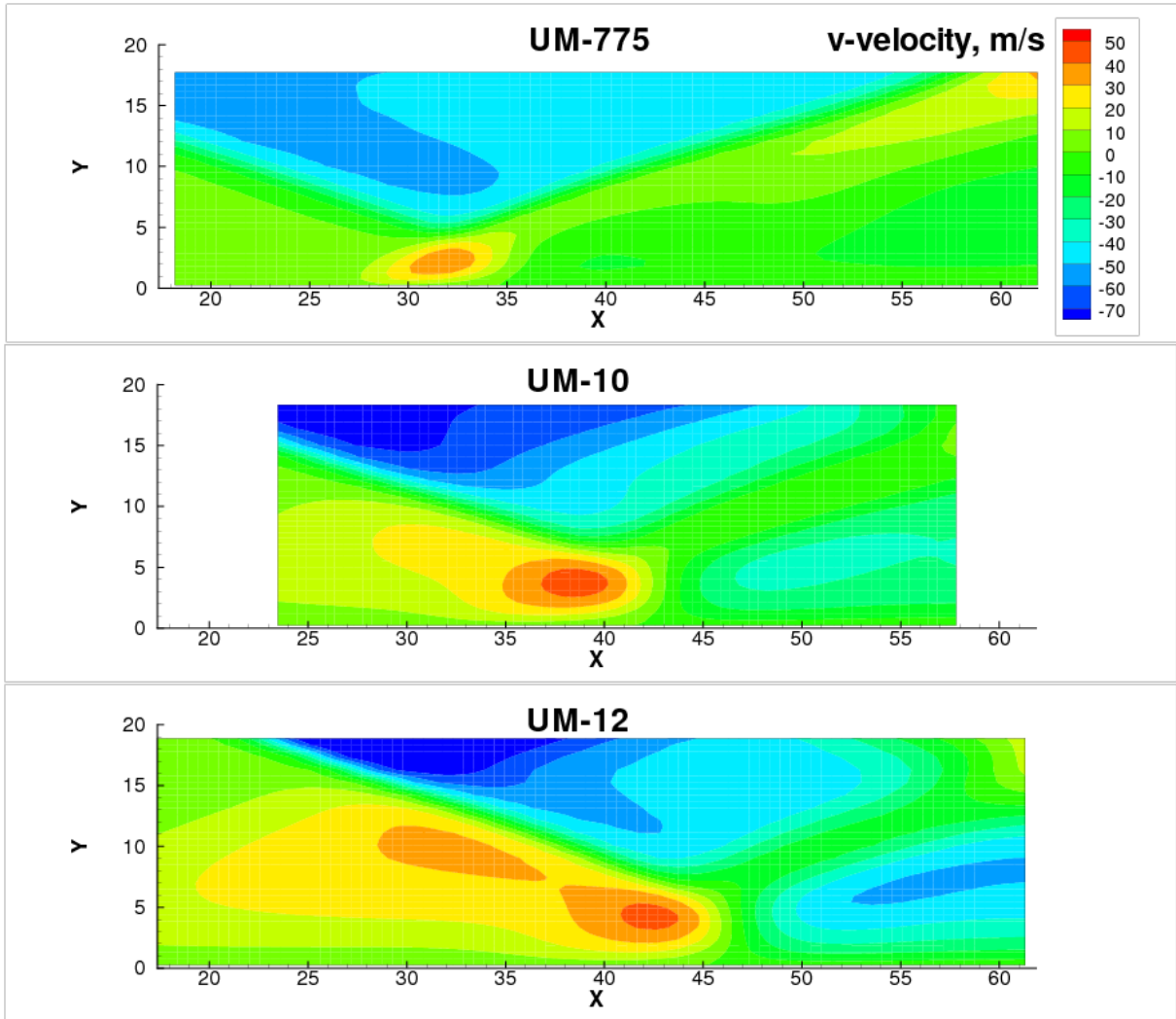
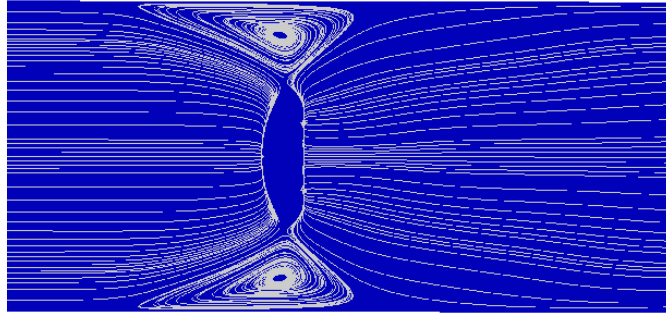
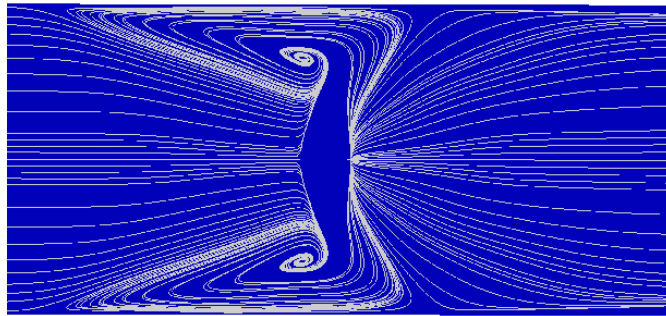


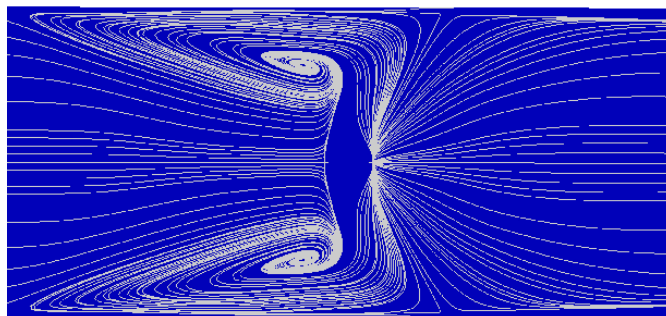
Figure 22. Comparison of centerplane CFD fine-grid v -velocity contours for all three CCAS cases (CFD results from fine grid have been interpolated to PIV grid points).



(a) $\theta = 7.75^\circ$



(b) $\theta = 10.0^\circ$



(c) $\theta = 12.0^\circ$

Figure 23. CFD bottom wall surface-restricted streamlines in the interaction region for all three CCAS cases on fine grids (flow is from left to right).

REPORT DOCUMENTATION PAGE

*Form Approved
OMB No. 0704-0188*

The public reporting burden for this collection of information is estimated to average 1 hour per response, including the time for reviewing instructions, searching existing data sources, gathering and maintaining the data needed, and completing and reviewing the collection of information. Send comments regarding this burden estimate or any other aspect of this collection of information, including suggestions for reducing this burden, to Department of Defense, Washington Headquarters Services, Directorate for Information Operations and Reports (0704-0188), 1215 Jefferson Davis Highway, Suite 1204, Arlington, VA 22202-4302. Respondents should be aware that notwithstanding any other provision of law, no person shall be subject to any penalty for failing to comply with a collection of information if it does not display a currently valid OMB control number.
PLEASE DO NOT RETURN YOUR FORM TO THE ABOVE ADDRESS.

1. REPORT DATE (DD-MM-YYYY) 01-10-2010		2. REPORT TYPE Technical Memorandum		3. DATES COVERED (From - To)	
4. TITLE AND SUBTITLE CFL3D Contribution to the AIAA Supersonic Shock Boundary Layer Interaction Workshop				5a. CONTRACT NUMBER	
				5b. GRANT NUMBER	
				5c. PROGRAM ELEMENT NUMBER	
				5d. PROJECT NUMBER	
6. AUTHOR(S) Rumsey, C. L.				5e. TASK NUMBER	
				5f. WORK UNIT NUMBER 561581.02.08.07.20.14	
				8. PERFORMING ORGANIZATION REPORT NUMBER L-19922	
7. PERFORMING ORGANIZATION NAME(S) AND ADDRESS(ES) NASA Langley Research Center Hampton, VA 23681-2199				10. SPONSOR/MONITOR'S ACRONYM(S) NASA	
9. SPONSORING/MONITORING AGENCY NAME(S) AND ADDRESS(ES) National Aeronautics and Space Administration Washington, DC 20546-0001				11. SPONSOR/MONITOR'S REPORT NUMBER(S) NASA/TM-2010-216858	
12. DISTRIBUTION/AVAILABILITY STATEMENT Unclassified - Unlimited Subject Category 02 Availability: NASA CASI (443) 757-5802					
13. SUPPLEMENTARY NOTES					
14. ABSTRACT This paper documents the CFL3D contribution to the AIAA Supersonic Shock Boundary Layer Interaction Workshop, held in Orlando, Florida in January 2010. CFL3D is a Reynolds-averaged Navier-Stokes code. Four shock boundary layer interaction cases are computed using a one-equation turbulence model widely used for other aerodynamic problems of interest. Two of the cases have experimental data available at the workshop, and two of the cases do not. The effect of grid, flux scheme, and thin-layer approximation are investigated. Comparisons are made to the available experimental data. All four cases exhibit strong three-dimensional behavior in and near the interaction regions, resulting from influences of the tunnel side-walls.					
15. SUBJECT TERMS Shock; Boundary layer; Supersonic					
16. SECURITY CLASSIFICATION OF:			17. LIMITATION OF ABSTRACT	18. NUMBER OF PAGES	19a. NAME OF RESPONSIBLE PERSON
a. REPORT	b. ABSTRACT	c. THIS PAGE			STI Help Desk (email: help@sti.nasa.gov)
U	U	U	UU	36	19b. TELEPHONE NUMBER (Include area code) (443) 757-5802

